NRC Research Press

ARTICLE

Seismic reliability of axially loaded vertical piles

Gennaro Esposito, Gordon A. Fenton, and Farzaneh Naghibi

Abstract: The reliability of single vertical pile foundations subjected to seismic loads is assessed and compared with the minimum acceptable reliability level for static load conditions mandated by the Canadian codes. The analysis is executed for a site with a mean shear-wave velocity of the top 30 m of the ground equal to 250 m/s subjected to the ground motion hazard of five Canadian cities. Using both a full probabilistic analysis and simplified probabilistic model, the results seem to indicate that the current design practice is unable to achieve the reliability target of the codes. The shortfall is particularly significant when the limiting pile settlement is relatively small. The calculated reliability level of small limiting settlements is impacted by the geotechnical variability, whereas the seismic hazard variability affects large pile limiting settlements. Finally, the simplified probabilistic model produces the same results as the full probabilistic model for large pile settlement and is a convenient tool to execute code calibration.

Key words: seismic reliability, pile foundations, seismic settlements, seismic hazard.

Résumé : Le degré de fiabilité des fondations sur pieux verticaux simples sous charge sismique a été évalué et comparé au niveau de fiabilité minimum acceptable pour les conditions de charge statique prescrit par les codes canadiens. La présente analyse est effectuée pour un site dont la vitesse de l'onde de cisaillement moyenne des 30 premiers mètres du sol est égale à 250 m/s et qui est exposé au risque de mouvement du sol de cinq villes canadiennes. En appliquant à la fois une analyse probabiliste complète et un modèle probabiliste simplifié, il semble que les conclusions révèlent que les pratiques de conception actuelles ne permettent pas d'atteindre l'objectif de fiabilité des codes. Le déficit est particulièrement important lorsque le tassement limite des pieux est relativement faible. Les variations géotechniques influent sur le niveau de fiabilité calculé pour les petits tassements limites, tandis que les variations liées aux aléas sismiques ont une incidence sur les grands tassements limites des pieux. Pour conclure, les résultats du modèle probabiliste simplifié sont les mêmes que ceux du modèle probabiliste complet pour les grands tassements de pieux et constituent un outil pratique pour l'étalonnage du code. [Traduit par la Rédaction]

Mots-clés : fiabilité sismique, fondations de la pile, implantations sismiques, risque sismique.

Introduction

In the "load and resistance factor design" (LRFD) format, the characteristic value of the geotechnical resistance of pile foundations is multiplied by a factor — the geotechnical resistance factor, φ — to obtain the design value of the geotechnical resistance (Fenton et al. 2016). Geotechnical resistance factors, φ, typically <1, are intended to scale the geotechnical resistance to values sufficiently small to achieve the desired design target reliability index, β, which represents the minimum level of performance expected from a geotechnical system and depends on personal and societal safety requirements, aversion to potential losses, and amount of investments necessary to improve safety. The geotechnical resistance factors, φ, are obtained through calibration, which is the probabilistic calculation of factors to be applied to all the quantities used in the design process. For instance, the Canadian Highway Bridge Design Code (CHBDC; CSA 2014) adopts a set of geotechnical resistance factors for axially loaded pile foundations subjected to dead and live load actions, which were derived through rigorous calibration.

For vertical axially loaded pile foundations subjected to seismic loads, the geotechnical resistance factors given in codes are often based on empirical considerations and the actual reliability level during the design life is currently unknown. As a consequence of the lack of rigorous calibration, codes in different jurisdictions provide very different geotechnical resistance factors. The inability to estimate the reliability level achieved by pile foundations subjected to seismic loads not only complicates the quantification of the vulnerability of foundations and their supported structures, but also limits estimation of possible monetary loss deriving from partial damage or total loss of a structure due to an earthquake.

In this paper, the reliability level achieved by axially loaded vertical pile foundations subjected to seismic load is investigated considering the Canadian seismic hazard levels (NRCan 2015) and the National Building Code of Canada (NBC) provisions (NRC 2015). Considering the reliability targets adopted for the design of geotechnical systems under relatively static dead and live loads, the goal of this paper is to investigate if the seismic geotechnical design according to the Canadian code achieves similar reliability levels as those aimed at by static design over the design life. There should be no satisfactory reason to accept differing target safety levels (and thus reliability) for a geotechnical system designed to resist both static and seismic loads. After introducing the geotechnical seismic reliability framework, the pile seismic reliability is assessed for five major Canadian cities using a performance-based approach. In addition, a simplified probabilistic model is introduced that can be used to estimate the pile seismic reliability for code calibration. Observations and recommendations for further research are provided.

Received 29 May 2019. Accepted 10 January 2020.

G. Esposito.* Projects and Engineering Services, Shell Global Solutions, 400 – 4th Avenue SW, Calgary, AB T2P 0J4, Canada.
G.A. Fenton and F. Naghibi. Department of Engineering Mathematics and Internetworking, Dalhousie University, Halifax, NS B3J 2X4, Canada.
Corresponding author: Gennaro Esposito (email: Gennaro.Esposito@dal.ca).
*Present address: Department of Engineering Mathematics and Internetworking, Dalhousie University, Halifax, NS B3J 2X4, Canada.

Current seismic pile design and performance requirements

A review of available geotechnical codes reveals that seismic design of axially loaded vertical piles is quite inconsistent among countries and jurisdiction. The authors assume that any geotechnical code seismic provisions target safety provisions (e.g., extreme and ultimate limit states) corresponding to initiation of structural collapse. Under these premises, in many cases codes allow the pile foundation to be loaded close to the ultimate foundation resistance, therefore allowing resistance factors higher than those under static conditions and sometimes as high as 1.0 (CSA 2014; Oregon Department of Transportation 2018; AASHTO 2017). The most recent version of the CHBDC (CSA 2019) prescribes seismic geotechnical resistance factors equal to one for capacity-protected elements and performance-based design, equal to the static resistance factors plus 0.2 for force-based design elements. On the other end of the spectrum, Eurocode 8 (CEN 2004*b*), based on the partial material factor approach, instead recommends for the seismic design case the same geotechnical material factors recommended in Eurocode 7 (CEN 2004*a*) for the static case. There seems to be no consensus in the geotechnical community on the target reliability level for seismic design of pile foundations.

In addition to differing design guidance, there seems to be little research on the seismic reliability of axially loaded vertical piles, most of the available seismic design literature focusses on laterally loaded piles. The subject of foundation seismic reliability is relatively new and only recently, Naghibi and Fenton (2019) have developed a methodology to estimate geotechnical resistance factors for shallow foundations subjected to seismic loads. The results of their paper suggested that resistance factors should be lower than currently used in Canadian practice, and possibly lower than the static ones depending on hazard and variability of the soil conditions. The methodology developed by Naghibi and Fenton (2019) is applied in this study and expanded to pile foundations. Honjo et al (2004), using an extreme value distribution, estimated the geotechnical resistance factor for vertical piles under axial loads and determined that the resistance factor for the seismic case and a return period of 2475 years should be 0.63. Kramer et al. (2014) tried to develop a performance-based framework for bridge pile group foundations considering all potential levels of loading and their likelihoods of occurrence. Their study indicated that the resistance factors for large groups of piles generally decreased as the return period increased and varied from just less than one at very short return periods to between 0.8 and 0.9 at very long return periods.

The Task Force Report for the Greater Vancouver Region (Anderson et al. 2007) provides guidance on the maximum acceptable settlements caused by soil softening due to seismic loading for buildings designed according to the 2005 version of the NBC (NRC 2005). Guidance provided by the Task Force (Anderson et al. 2007) is based on the vertical drift ratio, defined as the difference in vertical displacement of a column relative to an adjacent column divided by the column spacing. Vertical drift ratio limits are related to the horizontal drift limits given in the NBC (NRC 2005), which are defined as the difference between horizontal displacements of adjacent floors divided by the height between floors. The vertical drift ratio should not exceed 80% of the horizontal drift ratio. Table 1 shows the vertical drift ratio limits recommended by the Task Force (Anderson et al. 2007) for two earthquake levels. The differential settlements between two pile-supported columns is often taken as approximately half of the total settlement, assuming that the piles are predicted to have approximately the same total settlement. From Table 1, for a post-disaster building that is allowed a 0.8% maximum vertical drift ratio limit with, say, a 10 m bay size or 10 m span, the allowable maximum vertical differential deflection would then be 80 mm at 2475 years return period and 60 mm at 475 years return period. The Task Force Report (Anderson et al. 2007) does not specify the reliability levels associated with the vertical drift ratio limits.

Table 1. Vertical drift ratio limits from the Task Force report (Anderson et al. 2007).

	Vertical drift ratio limit (%)	
Importance category	Return period 2475 years	Return period 475 years
Post-disaster importance	0.8	0.6
High importance	1.6	1.2
Normal importance	2.0	1.5

Pile seismic performance

Figure 1 shows the static and two seismic load–settlement curves of a 900 mm diameter driven steel pipe pile, the latter two curves representing small liquefaction (for instance, the softening of the top layer) and larger wide-spread liquefaction. In this paper, the term liquefaction is used broadly to indicate the whole spectrum of immediate earthquake effects on the soil resistance, ranging from softening to the complete loss of strength. Under static conditions, the pile is designed to experience "small" settlements corresponding to relatively elastic conditions under the design load, where "small" typically means equal to or less than a serviceability design value, z_{des} (Fig. 1), generally corresponding to the serviceability limit state (SLS) unfactored axial load, L_{des}. The ultimate settlement, z_{ult}, and the corresponding ultimate pile axial capacity, L_{ult} (Fig. 1), are associated with the ultimate limit state (ULS) of the piles and are typically determined using empirical or semi-empirical methods. In this study, the ultimate capacity is assumed to be the axial load at the settlement z_{ult} (Fig. 1) corresponding to 10% of the pile diameter. In Fig. 1, z_{fail} is the unacceptable settlement causing initiation of damage to the superstructure (failure settlement) and z_{seis} is the seismic-induced settlement caused by decrease in soil strength and stiffness and by the additional inertial load (seismic settlement). It is important to note that z_{fail} and z_{ult} are not identical and that z_{fail} can be much smaller than z_{ult} depending on the definition of damage. Also note that in geotechnical design practice, the settlement at failure, z_{fail}, is not typically defined and the pile seismic design often relies on a force balance approach. In this study, z_{fail} has a broad meaning, as it could be the settlement causing unrepairable damage and initiation of collapse, thus related to ULS and the vertical drift limits in Table 1 (Anderson et al. 2007), as well as the settlement related to serviceability damage.

Pile seismic reliability

The earthquake ground motion causing soil liquefaction is usually characterized by the hazard function relating the intensity level of the ground motion, $A = a$, to the annual mean rate of exceedance (MRE) or alternatively to the mean return period (MRP). The MRP is defined as the reciprocal of the annual MRE, and in this paper MRP and MRE are used interchangeably. Throughout this paper, the peak ground acceleration (PGA) is used as the ground motion intensity measure A. For instance, Fig. 2 shows the MRE of A for the city of Vancouver taken from the Natural Resources Canada seismic hazard calculator website (NRCan 2015). For small ground motion intensities of engineering interest, the rare-event assumption holds (Bazzurro and Cornell 2004*b*), which means that the likelihood of two or more events occurring in the period of interest is small in comparison to the likelihood that one event happens. The rare-event assumption implies that the MRE of a value $A = a$ is numerically equal to the probability that the annual maximum ground motion intensity exceeds a. As MREs are rates and can exceed 1, while complementary cumulative distribution functions (CCDFs) represent proba-

Fig. 1. Load–settlement curves of 900 mm diameter driven steel pipe pile.

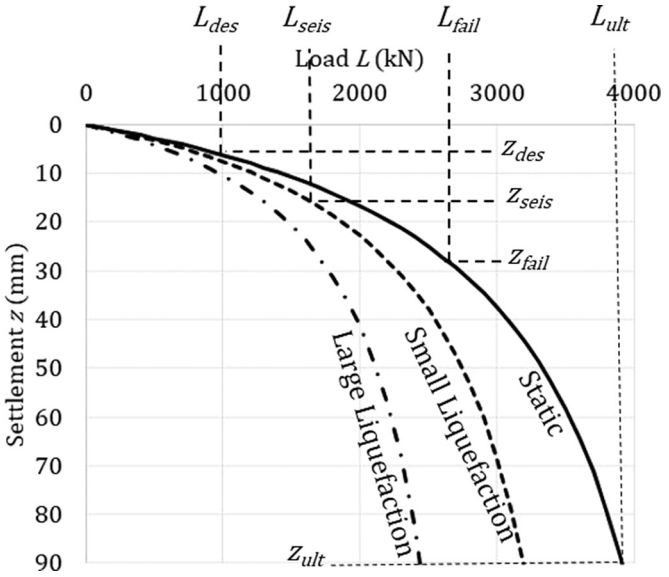

bilities and cannot exceed 1, in this paper the MRE is truncated from the seismic hazard calculator (NRCan 2015) at 1, implying that very small ground motion intensities can occur only once a year or less. From this assumption, it follows that the hazard or MRE curve, like the one in Fig. 2, is numerically identical to the CCDF of A, H_A. From this, it also follows that the cumulative distribution function (CDF) of A, $F_A(a)$, is simply $1 - H_A(a)$ and the probability density function (PDF) of A is

$$(1) \qquad f_A(a) = \frac{d[1 - H_A(a)]}{da}$$

Given the significant uncertainties in ground motion estimates, a proper probabilistic seismic hazard evaluation must include the variability of the selected ground motion parameters A at all exceedance probabilities. The variability of A includes both epistemic and aleatory uncertainty and is represented in Fig. 2 by the mean μ_H plus/minus one standard deviation σ_H (dashed lines).

For axially loaded vertical piles, it is convenient to formulate the reliability problem in terms of the maximum allowable settlement, Z_{fail}, the capacity related to the limits described in the previous section (Anderson et al. 2007; NRC 2015), and the seismic-induced settlement, Z_{seis}. Z_{seis} is a random variable with mean $\mu_{Z,seis}$ and standard deviation $\sigma_{Z,seis}$ that depends on the random ground motion and soil properties. Z_{fail} is also a random variable as the settlement at which, for instance, structural repair becomes necessary may well vary from structure to structure (Cornell 1996). Nevertheless, the variability of Z_{fail} is much less than the variability of Z_{seis}, and so it is reasonable to simplify the reliability problem by assuming that Z_{fail} is a deterministic value, derived for instance from Table 1 (Anderson et al. 2007). Assuming that Z_{seis} is lognormally distributed, the pile limit state function, Z, can be expressed as

$$(2) \qquad \ln(Z) = \ln(Z_{fail}/Z_{seis})$$

where Z is also lognormally distributed with mean μ_Z and standard deviation σ_Z. The pile probability of failure is the probability that $\ln(Z) < 0$. Figure 3 shows the relationship between $Z = z$ and the ground motion intensity $A = a$. As a increases, z decreases as a result of soil liquefaction and the additional inertial load acting on the pile. Figure 3 also shows the PDF of z, $f_z(z|a)$, at a certain ground motion intensity $A = a$. At that ground motion intensity, the probability of pile failure $P_{f,a}$ (shaded area under the PDF), conditional to the occurrence of $A = a$, is

$$(3) \qquad P_{f,a}(a) = P[Z < 0|A = a] = \int_0^1 f_Z(z|a)\, dz = F_{Z,a}(1)$$

where P[] indicates the probability of the event and $F_{z,a}(1)$ is the CDF of Z at $A = a$. If eq. (3) is applied to all possible ground motion intensities $A = a$ impacting the pile, the fit to the resulting collection of conditional probabilities of failures is the fragility function, $F_z(a)$. $F_z(a)$ represents the capacity of the geotechnical system and is often assumed to be lognormally distributed — see, for instance, guidance in ASCE 7-16 (ASCE 2016) for structural systems or Argyroudisa et al. (2013) for geotechnical systems — and its CDF can then be estimated as

$$(4) \qquad F_Z(a) = \Phi\left[\frac{\ln(a/\mu_{\ln Z})}{\sigma_{\ln Z}}\right]$$

where $\Phi[]$ is the standard normal CDF, $\sigma_{\ln z}$ is the standard deviation of the natural logarithm of the pile limit state function Z, and $\mu_{\ln z}$ is the mean of the natural logarithm of Z measured in the same units as a. As $f_A(a)$ is the PDF of the event that the ground motion $A = a$ in 1 year, the convolution integral of $F_z(a)$ and $f_A(a)$ for every $A = a$ represents the pile's annual unconditional probability of failure, $P_{f,1}$

$$(5) \qquad P_{f,1} = \int_0^\infty F_Z(a)P[A = a] = \int_0^\infty F_Z(a)f_A(a)\, da$$

In other words, $P_{f,1}$ is the annual total probability that the demand Z_{seis} exceeds the capacity Z_{fail} for any possible ground motion $A = a$ at a given location. It is interesting to note that in the standard of practice, only selected ground motion intensities are used to check the seismic performance. For instance, the Task Force report (Anderson et al. 2007) provides settlement limits for two ground motions only. Therefore, the seismic-induced settlement check against the values in Table 1 represents only the pile failure conditional to the occurrence of the chosen two ground motions rather than all possible ground motions.

Methodology to determine pile reliability

In performance-based seismic design, a structure is designed for inertial loading effects associated with the dynamic response of the structure. Some structures may also experience seismically induced kinematic effects, associated with soil liquefaction and lateral spreading. Modelling the combination of inertial and kinematic earthquake effects is not an easy task and is usually done through three simplified methodologies; namely, the superposition of results, post-inertial kinematic response, and post-kinematic inertial response. Galbraith et al. (2018) presents a comprehensive review of the three methodologies. In this study, the post-kinematic inertial approach is applied, where kinematic effects, e.g., softening or liquefaction, are applied prior to the occurrence of the inertial demand through use of a soil model representative of softened conditions. Also, any lateral kinematic displacements (or pressures) that could impact the structural stability of the piles and any post-seismic consolidation settlement are ignored. The inertial pseudo-static pile response is then started from the end of the kinematic effects. The post-kinematic combination method is

Fig. 2. Seismic hazard for city of Vancouver.

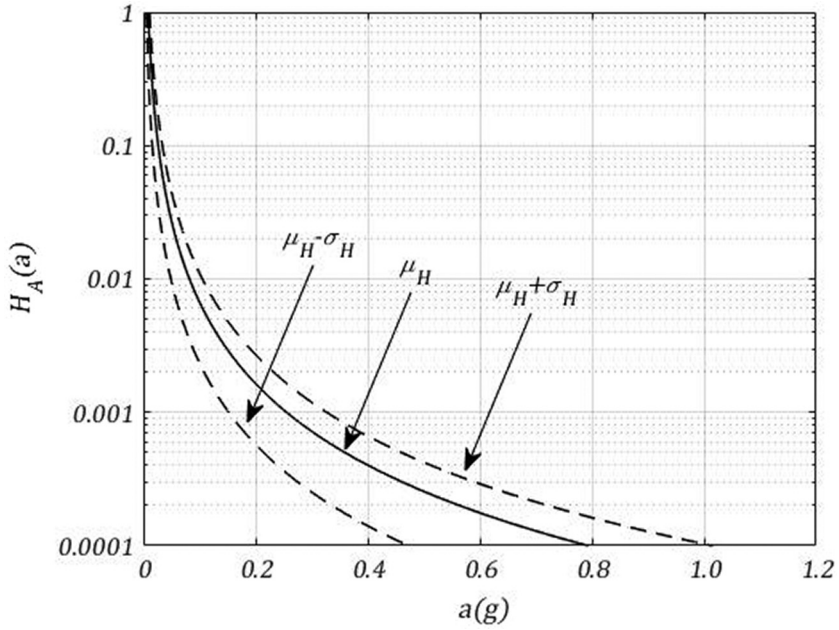

Fig. 3. Relationship between settlements and ground motion intensity.

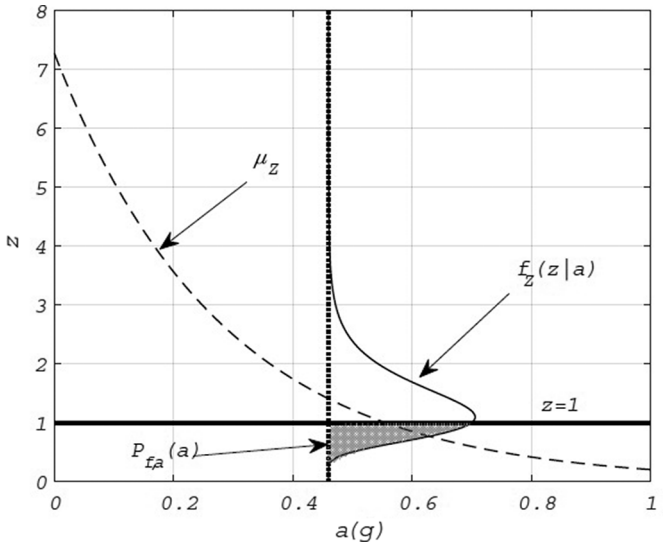

simpler to use than other approaches and provides results that represent the actual behaviour reasonably well, short of performing numerous dynamic time-history models (Galbraith et al. 2018). However, the interpretation of the results requires understanding of the limits in the applicability of the modelling. First, the PGA (and associated maximum inertial load) is not concurrent with the maximum excess pore pressure and the minimum soil strength. The second important limitation is an inability to model the pile damage caused by inertial and kinematic conditions, which can alter the pile axial capacity. While plastic hinges caused by inertial loads may form at the connection between the pile and superstructure, kinematic hinges usually form in the soil just below the softened layer, where the stiffness of the underlying nonsoftened soil may be significantly higher than the softened layer. In this study, the structural integrity of the pile is assumed unaffected by inertial and kinematic conditions. Note that in this study, "static" is used to indicate pile foundations subjected to dead and live loads and "seismic" to indicate pile foundations subjected to inertial loads and kinematic conditions in addition to dead and live loads, in approximate alignment with the load combinations given in the NBC (NRC 2015) (i.e., for companion loads, full live load is applied, but snow load is ignored). In addition, the CHBDC (CSA 2014) is followed to characterize the geotechnical resistance and design the piles. The following steps are followed to assess the seismic reliability of piles:

1. The uniform ground motion hazards for sites at five Canadian cities — Montreal, Ottawa, Toronto, Vancouver, and Victoria — are obtained from the Natural Resources Canada seismic hazard calculator website (NRCan 2015).
2. Using an equivalent nonlinear site response model, the cyclic stress ratio at a site characterized by 30 m of silty sand is used to estimate the pore pressure increase during shaking caused by the five different ground motion hazards.
3. The initial (static) and increased (seismic) pore pressure during shaking are used to calculate the soil's effective vertical stress during the seismic event at each site.
4. A pile type (driven or bored) and a cross section are selected.
5. The maximum allowable settlement, Z_{fail}, is chosen for a given damage state, e.g., 5% of the pile diameter.
6. Assuming that a semi-empirical analysis using laboratory and in situ data is used to estimate the geotechnical pile capacity, following CHBDC (CSA 2014) the geotechnical resistance factor is selected to be 0.4. Also, an importance factor of 1.0 is selected.
7. Under static conditions for the chosen pile type and cross section, the ULS load combination 3 (NRC 2015) is used to choose the pile length; the static load–settlement curve is then calculated.
8. Under seismic conditions, a modified version of ULS load combination 5 (NRC 2015) is used to determine the load acting on the pile under the ground motion $A = a$; the modified load combination includes full dead and live loads and ignores the snow load. The possible occurrence of snow load during the seismic event is ignored in the NBC (NRC 2015), and is consequently also ignored in this study, although this may be somewhat unconservative. The modified load combination is used to calculate the seismic load–settlement curve and to determine Z_{seis}.

Fig. 4. Soil conditions considered in this study.

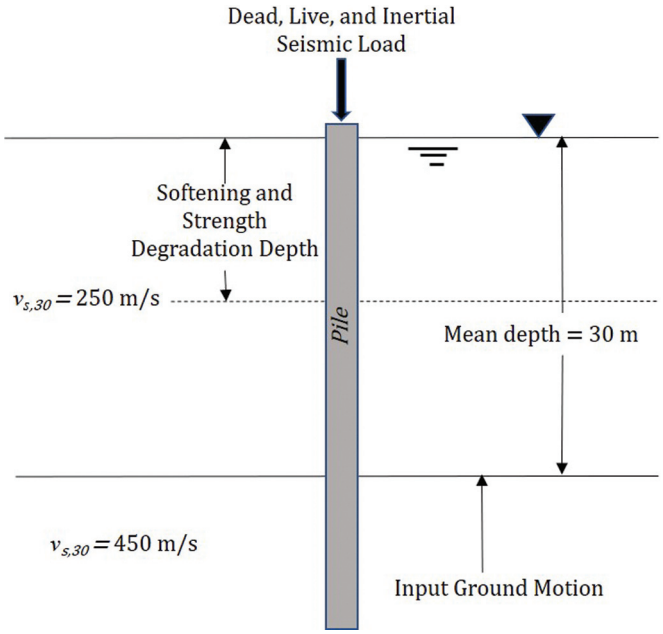

9. The probability that the pile limit state $\ln(Z) = \ln(Z_{fail}/Z_{seis})$ is less than 0 (failure) for this specific pile is determined for a selected ground motion $A = a$.
10. The procedure above is repeated for different ground motion values so that the fragility functions (eq. (4)) can be estimated for this pile type.
11. The unconditional probability of failure, $P_{f,1}$, is calculated through eq. (5).

The steps above are discussed in the following sections.

Site conditions and ground motion hazard

To assess the reliability of piles designed according to the Canadian codes, a single pile subjected to axial load (Fig. 4) installed in a surficial soil deposit (NRC 2015) which rests on a more competent deeper soil layer is considered in this paper. The surficial deposit is a silty sand with fines content (FC) of 15% and cyclic response similar to the soils considered in Cubrinovski and Rees (2008). In this example, the surficial deposit has a mean thickness of 30 m; mean shear-wave velocity, $v_{s,30}$, of 250 m/s; and minimum and maximum void ratio equal to 0.55 and 1.1, respectively. The deeper competent layer has a mean shear-wave velocity of 450 m/s. The shear-wave velocities and the average geometry of the soil layers correspond to the values used to determine the site coefficients adopted in the Canadian codes (Humar 2015; NRC 2015; CSA 2014). The mean fundamental period of the example site is assumed to be 0.48 s and the water table is assumed conservatively to be at ground surface. It is believed that the chosen site conservatively represents conditions common to many regions in Canada.

The example site described above is subjected to the ground motion hazards of the five locations considered in this study. To create continuous hazard curves covering the ground motion of interest, this study follows the approximation recommended by NRCan (2015) and uses a log–log scale and a linear regression to fit the discrete ground motion values a, expressed in terms of gravitational acceleration g, and the corresponding MRE from the NRCan (2015) hazard calculator

$$\ln(\text{MRE}) = \ln(H_A) = k_{a,1}\ln(a) + k_{a,2} \quad (6)$$

The regression, with the ground motion hazard extrapolated to MRE equal to 10 000 years, is shown in Fig. 5 while the coefficients and standard deviations of the regression are presented in Table 2. Note that the regression model in eq. (6) is different than the regression model recently adopted by Naghibi and Fenton (2019) and slightly overestimates the ground motion at very low MREs, as also suggested by NRCan (2015). Nevertheless, eq. (6) is used in this study for its simplicity and alignment with the standard of practice.

The fifth generation of the Canadian seismic hazard model (Adams et al. 2015) provides the mean values of the ground motion at the MRP of engineering interest. The output of the National Seismic Hazard Model (NRCan 2015) is affected by source, propagation, and attenuation uncertainty, which is to be accounted for in a reliability calculation. S. Halchuk and J.G. Adams (personal communication, 2018) provided the percentile distributions of the ground motion A for the five Canadian cities considered in this study at the MRP of 2475 years (MRE of 0.000 404 per annum). These percentile distributions are fitted to lognormal distributions to derive the statistics of the hazard model. Figure 6 shows the results of the regression while Table 3 shows the mean, median, standard deviation, and coefficient of variation (COV). The PGA $\text{COV}_{A,2475}$ values for the 2475 year MRP range from 64% in Victoria to 84% in Toronto. In this study, the PGA $\text{COV}_{A,2475}$ is assumed to remain constant for all MRP at the same location. For instance, in Victoria, the $\text{COV}_{A,500}$ for MRP equal to 500 years is assumed to be equal to $\text{COV}_{A,2475}$ = 64%. The impact of this assumption will be discussed later.

Site response

Equivalent-linear site response is utilized to model site response by means of the software Strata, based on Random Vibration Theory (RVT; Kottke and Rathje 2008) and one-dimensional (1-D) simulation of the soil variability over depth (Toro 1995). The mean uniform hazard spectrum for each location obtained from the hazard calculator of NRCan (2015) is used as input motion at the boundary between the more competent soil and the surficial silty sand deposit (Fig. 4). The surficial silty sand deposit is discretized into 10 sublayers. At each location, the mean hazard spectrum is applied to several realizations of the soil properties derived through Monte Carlo simulations. The random properties of the soil are derived through a layering model and a velocity model. The first models the layering thickness as a nonhomogeneous Poisson process where the rate changes with depth $\lambda(d)$, where d is depth from the ground surface, as

$$\lambda(d) = k_{d,1}(d + k_{d,2})^{k_{d,3}} \quad (7)$$

where the coefficients $k_{d,1}$, $k_{d,2}$, and $k_{d,3}$ are 1.53, 11.22, and –1.05, respectively, and are estimated using the method of maximum likelihood applied to the layering measured at 38 sites close to the locations considered in this study. The occurrence rate $\lambda(d)$ decreases as the depth increases whereas the expected thickness of deeper layers increases. The expected layer thickness, h, is equal to the inverse of the occurrence rate ($h = 1/\lambda(d)$). In addition to eq. (7), the modelled layer thickness, h, is also controlled by the maximum frequency to be transmitted through the soil column, which together with shear-wave velocity effectively controls the modelled thickness. This simplified model is expected to produce a reasonable approximation of the actual soil layer discretization as the rate of change of soil properties usually decreases with depth.

After the layering of the profile has been established, the density, shear-wave velocity, and damping profiles can be generated by assigning random velocities and damping at mid-depth of each layer and assuming that they are log-normally distributed. The

Fig. 5. Mean PGA hazard curves for the five locations considered in this study.

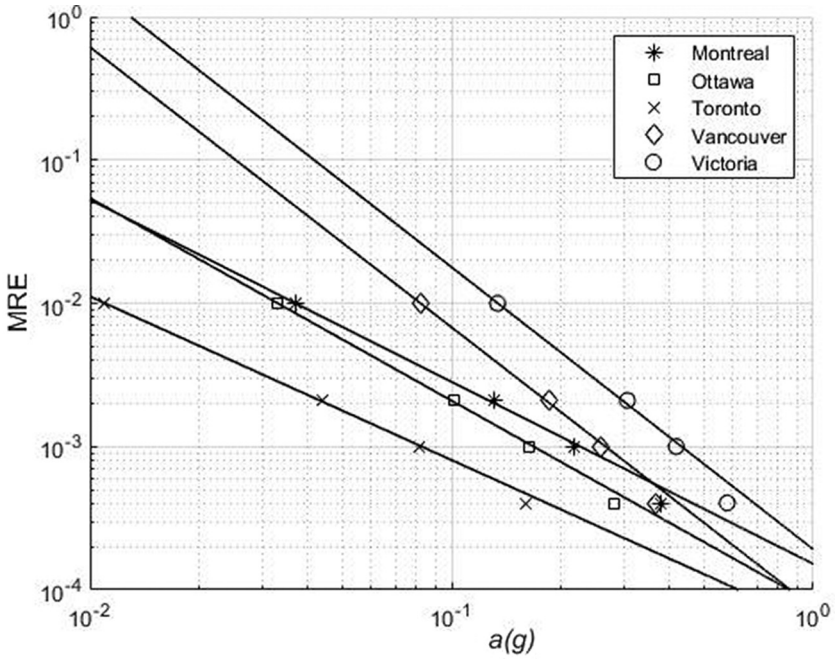

Table 2. Coefficients of the regression model in eq. (6).

	Montreal	Ottawa	Toronto	Vancouver	Victoria
$k_{a,1}$	–1.3652	–1.489	–1.1907	–2.119	–2.1553
$k_{a,2}$	–9.045	–9.6404	–9.9392	–9.8214	–8.8597
$\sigma_{A,\text{fit}}$	1.20E–03	7.90E–04	7.1E-04	1.37E–03	1.49E–03

Table 3. Ground motion statistics for 2475 year MRP.

	Mean (g)	Median (g)	$\sigma_{A,2475}$ (g)	$\text{COV}_{A,2475}$ (%)
Montreal	0.31	0.25	0.23	76
Ottawa	0.24	0.20	0.17	72
Toronto	0.13	0.09	0.11	84
Vancouver	0.32	0.29	0.21	65
Victoria	0.52	0.49	0.33	64

Fig. 6. Variability of A from National Seismic Hazard Model (NRCan 2015) at 2475 MRP.

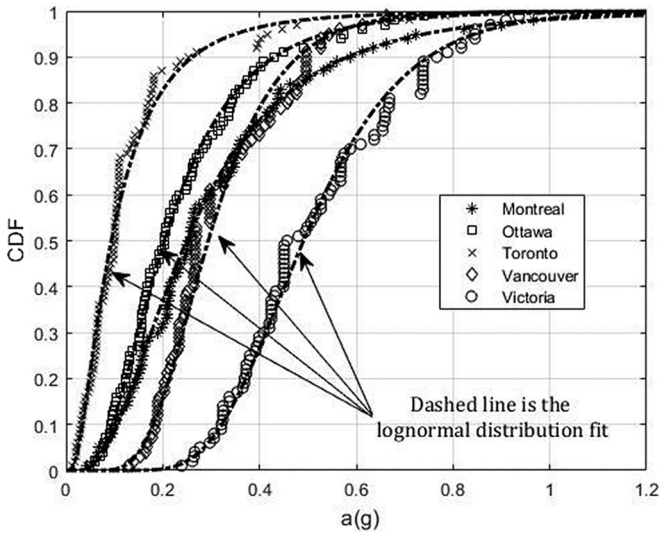

resulting standard normal variable S_i of the property X (density, shear-wave velocity or damping) of the ith layer is

$$S_i = \frac{\ln X_i - \mu_{\ln X}}{\sigma_{\ln X}} \quad (8)$$

where X_i is the soil property in the ith layer; $\mu_{\ln X}$ and $\sigma_{\ln X}$ are the mean and the standard deviation of the natural logarithm of the soil property, respectively. Realizations of depth varying cross-correlated values of S_i are generated by first taking S_1 to be a sample from a standard normal distribution. Remaining deeper layer soil properties are simulated using an autoregressive correlation model for $i = 2, 3, \ldots, n$ as

$$S_i = \rho S_{i-1} + \varepsilon_i \sqrt{1 - \rho^2} \quad (9)$$

where ρ is the correlation coefficient between adjacent layers, S_{i-1} is the standard normal variable of the previous layer, and ε_i is a new standard normal random variable with zero mean and unit standard deviation. The soil layer properties are obtained through the transformation

$$X_i = \exp(\mu_{\ln X} + \sigma_{\ln X} S_i) \quad (10)$$

This procedure, with a COV of $\sigma_{\ln X}/\mu_{\ln X} = 0.2$ assigned to the uncertain soil properties, is adopted to generate realizations of the site. It is recognized that the above soil randomization procedure is a much less flexible representation of random fields as described in Fenton and Griffiths (2003) and recently applied for geotechnical seismic reliability (Naghibi and Fenton 2019). However, the simplified 1-D autoregressive model is considered sufficient for the scope of this research, which is to have a preliminary assessment of the effect of the ground motion variability and soil variability (much smaller than ground motion variability) on the pile reliability. Ten realizations of the site are produced from the simplified 1-D soil model, and this is considered sufficient to represent the intrasite variability as the ground motion variability

Table 4. Coefficients and standard deviations of regressions used to estimate r_u.

Term	$\sigma_{N_{eq}}$	$\sigma_{N_{liq}}$	b_1	b_2	b_3
WUS	0.64	0.31	−0.3643	−0.4105	0.2553
CEUS	0.66	0.31	0.4654	−0.5626	0.1423

has the largest impact on the site response (Bazzurro and Cornell 2004*a*).

At each location, the cyclic stress ratio (CSR) from the site response analysis is used to estimate the increase in pore-water pressure ratio, r_u, through correlations involving the number of equivalent cycles, N_{eq}, and the number of equivalent cycles to liquefaction, N_{liq}, originally proposed by Seed et al. (1975) and then revised by Green and Terri (2005). The pore water pressure ratio, r_u, is defined as

$$(11) \qquad r_u = \frac{u}{s'_v} \approx 0.5 + \frac{1}{\pi}\sin^{-1}\left[2\left(\frac{N_{eq}}{N_{liq}}\right)^{1/\alpha} - 1\right]$$

where u is the pore-water pressure, s'_v is the vertical effective stress, and the parameter α is an empirical constant estimated as (Polito et al. 2008)

$$(12) \qquad \alpha = c_0 + c_1(\mathrm{FC}) + c_2(\mathrm{Dr}) + c_3(\mathrm{CSR})$$

where FC is the fines content in percent; Dr is the relative density in percent; CSR is the cyclic stress ratio; and $c_0 = 0.5058$, $c_1 = 0.01166$, $c_2 = 0.007397$, and $c_3 = 0.01034$ are regression coefficients for FC < 35%, as given in Polito et al. (2008). After each realization, Dr is derived from the density and the minimum and maximum void ratio. The number of equivalent cycles, N_{eq}, is then estimated as (Lasley et al. 2017)

$$(13) \qquad N_{eq} = \exp[b_1 + b_2 \ln(a) + b_3 M_w + \delta_0]$$

where a is the peak ground acceleration in units of g at the surface of the soil profile; M_w is the moment magnitude of the earthquake in dynes/cm² (where 1 dyne = 10^{-5} N); b_1, b_2, and b_3 are regression coefficients; and δ_0 is an dimensionless residual term of the regression that includes the effect of the site variability and the ground motion variability. The numeric values of the coefficients and of the random term δ_0, assumed to be a zero-mean normally distributed random variable with standard deviations $\sigma_{N_{eq}}$, are presented in Table 4 (Lasley et al. 2017) for western United States (WUS — applied to Victoria and Vancouver) and for central-eastern United States (CEUS — applied to Toronto, Ottawa, and Montreal). Finally, N_{liq} is obtained from CSR and Dr derived from the site response analysis, using the N_{liq} versus CSR regressions given in Cubrinovski and Rees (2008) and Cubrinovski et al. (2010) for soil with FC < 20%. The numerical value of the regression standard deviation, $\sigma_{N_{liq}}$, is also shown in Table 4. With all the parameters needed for eq. (11), r_u profiles can be derived. Figure 7 shows the mean, μ_{r_u}, and mean plus/minus one standard deviation ($\mu_{r_u} + \sigma_{r_u}$ and $\mu_{r_u} - \sigma_{r_u}$) with depth d obtained after 10 realizations of r_u for the Vancouver ground motion hazard associated with MRP of 2475 years.

Pile axial capacity and load–settlement curves

During ground motion, the excess pore-water pressure results in momentary strength decrease and stiffness degradation of the surficial deposit. The extent of both depends on many factors, such as ground motion intensity, spectral characteristics, duration of the ground motion, and geometry of the deposits. The net result of the softening and strength degradation is a decrease of pile shaft resistance, which causes load redistribution along the pile and consequent additional settlements. The deeper layer shown in Fig. 4 does not liquefy and maintains most of its static strength and stiffness. This situation is quite common in practice and offers the opportunity to design piles sufficiently embedded in the no-liquefiable layer (Fig. 4) so that the possible effects of surficial liquefaction are mitigated by the stiffness and resistance of the deeper layer. Under static loading conditions, the geotechnical axial capacity of the pile, R, can be expressed as (Canadian Geotechnical Society 2006)

Fig. 7. Example of r_u profile caused by ground motion at Vancouver with MRP = 2475 years.

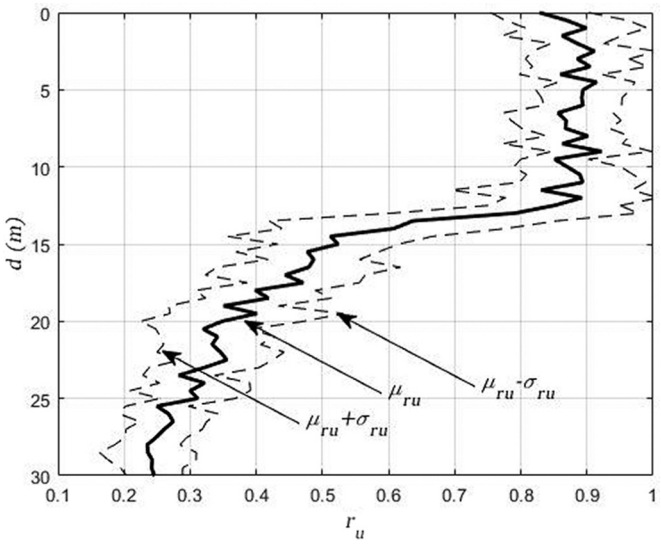

$$(14) \qquad R = \sum_{z=0}^{L_{pile}} C q_s \Delta z + A_t q_t - W_p$$

where L_{pile} is the pile length (m) subdivided into segments Δz (m), C is the pile circumference (m), q_s is the shear stress along the shaft (kPa), A_t is the pile toe area (m²), q_t the bearing capacity of the pile toe (kPa), and W_p is the pile weight (kN). For cohesionless soils, the shear stress along the shaft, q_s, and the bearing capacity of the pile toe, q_t, depend on the soil's vertical effective stress, s'_v, along the shaft and at the pile toe, respectively

$$(15) \qquad q_s = \beta_s s'_v$$

and

$$(16) \qquad q_t = N_t s'_v$$

where β_s and N_t are the shaft resistance factor and the bearing capacity factor, respectively, given in the Canadian Foundation Engineering Manual (Canadian Geotechnical Society 2006). During ground shaking, the seismic vertical effective stress, $\sigma'_{v,seis}$, decreases to

$$(17) \qquad s'_{v,seis} = s'_v(1 - r_u)$$

where r_u is the pore-water pressure ratio ranging from 0, for no excess pore pressure under static conditions, to 1, corresponding to complete liquefaction and resulting in $s'_{v,seis} = 0$ (see Fig. 7).

Fig. 8. (*a*) Relationship between *Z* and ground motion intensity *a* for driven steel pipe piles subjected to Vancouver ground motion hazard for a settlement z_{fail} = 5% of the pile diameter and (*b*) resulting fitted pile fragility curve shown as a solid line.

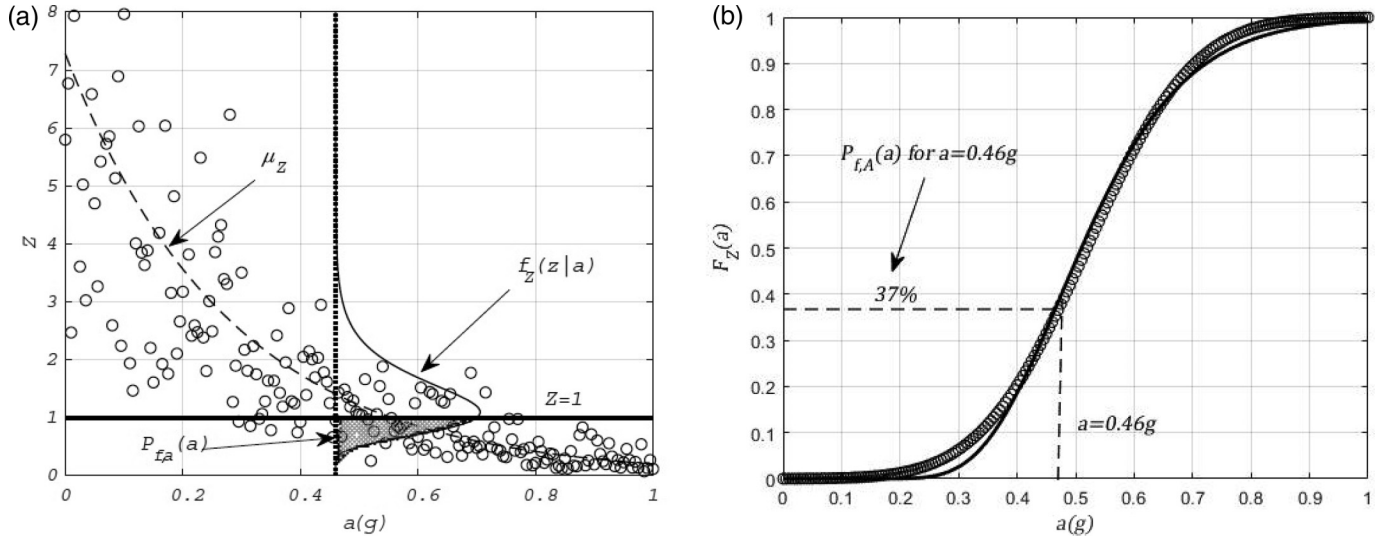

Replacing s'_v with $s'_{v,seis}$ in eqs. (15) and (16) allows the pile axial bearing capacity to be estimated under seismic conditions. With the static and seismic geotechnical pile axial capacities, the pile settlement is calculated using load-transfer ratios proposed by Reese and O'Neall (1988) for drilled shafts and from the method described in the Eurocode EN 1997-2 (CEN 2004*a*) and Dutch Standard NEN 6743 (Dutch Institute for Standardization 2006) for driven piles.

The total uncertainty of predicting the pile geotechnical capacity under static and seismic conditions consists of the following elements. The uncertainty in predicting the static geotechnical axial capacity with eq. (14) has a COV_R of 0.2 with a typical understanding of the soil conditions and the prediction model (Fenton et al. 2016). When calculating the seismic geotechnical axial capacity using eq. (17), the uncertainty in estimating r_u given in Table 4 needs to be added to the static uncertainty. Finally, the uncertainty in the load–settlement curves, $COV_{Z_{transfer}}$, derived from the load-transfer ratio is equal to 0.4 (Esposito 2017). Assuming that these uncertainty terms are uncorrelated, the above uncertainty can be added together to give $COV_{Z,seis}$ equal to 0.59.

Pile fragility

Having selected a failure settlement z_{fail}, e.g., 5% of the pile diameter, and after calculating z_{seis} using the geotechnical axial capacity and the load transfer ratios discussed earlier, it is possible to derive the pile limit state $\ln(Z) = \ln(Z_{fail}/Z_{seis})$ at the different ground motion intensities expected at a certain location. If this is repeated for different pile geometries and the resulting *Z* values are ordered as a function of the ground motion intensity *a*, relationships such as the one shown in Fig. 8*a* are obtained. The calculated *Z* values (circles) can be fitted with an exponential function, such as

$$Z = k_{Z,1} \exp(k_{Z,2} a) \quad (18)$$

where $k_{Z,1}$ and $k_{Z,2}$ are the coefficients of the regression. Figure 8*a* shows the regression of *Z*, representing the limit state of steel driven pipe piles subjected to the Vancouver ground motion hazard for a settlement z_{fail} equal to 5% of the pile diameter. Driven piles of diameter ranging from 400 to 910 mm and length ranging from 25 to 60 m were used to calculate the settlements and the resulting limit state *Z*. Figure 8*a* also shows the mean of *Z*, μ_Z, and the limit state corresponding to *Z* = 1, the failure point. Figure 8*a* indicates that as the ground motion intensity increases, the probability that *Z* < 1 increases and both μ_Z and the standard deviation of *Z*, $\sigma_{Z,fit}$, decrease. When the ground motion intensity increases, the variability of *Z*, expressed in terms of its coefficient of variation $COV_{Z,fit}$, which is the ratio of $\sigma_{Z,fit}$ and μ_Z, instead increases. This increase is caused by the higher probability of completely losing support from the surficial liquefiable layer which, in turn, increases the difference between settlements of long and short piles. The standard deviation $\sigma_{Z,fit}$ depends on the pile geometry variability (cross section and length) in addition to the soil resistance variability and the ground motion intensity. It is recognized that grouping piles of different geometry causes a large dispersion in the calculated *Z* values, as piles with long embedment in the lower nonliquefiable soil and larger diameter have very large *Z* values (z_{fail} much larger than z_{seis}), whereas piles with shorter embedment in the nonliquefiable deeper soil and smaller diameter have smaller *Z* values (z_{fail} approaching or less than z_{seis}). Despite the large variability, the relationship between *Z* and *a* can be still applied to adequately derive the pile fragility, provided that the standard deviation of *Z*, σ_Z, is explicitly accounted for when using eq. (4) to derive the fragility function $F_Z(a)$.

If at each ground motion intensity A = *a*, *Z* is assumed to be lognormally distributed (Fig. 8*a*), then the conditional probability $P_{f,a}(a)$ that the seismic-induced settlement z_{seis} exceeds the failure settlement z_{fail} can be calculated using eq. (3) as the probability that *Z* is <1. This probability is represented in Fig. 8*a* as the grey-shaded area. Computing eq. (3) for each possible ground motion intensity *A* = *a* results in a collection of conditional probabilities, $P_{f,a}(a)$, shown as circles in Fig. 8*b*. The collection of conditional probabilities, $P_{f,a}(a)$, can then be fitted with a lognormal distribution, eq. (4), to obtain the pile fragility function $F_Z(a)$, shown as a continuous curve in Fig. 8*b*. From the fragility function $F_Z(a)$, the probability of failure conditional to the occurrence of ground motion of a certain intensity can be determined. For instance, at *A* = 0.46*g*, Fig. 8*b* shows that the conditional probability of failure of steel driven pipe piles subjected to the Vancouver ground motion hazard for a settlement z_{fail} = 5% of the pile diameter is about 37%. Note that the standard deviation σ_Z of $F_Z(a)$ includes the uncertainty caused by several aspects, such as the standard deviation $\sigma_{A,RP}$ from the NRCan model (S. Halchuk and J.G. Adams, personal communication, 2018), the standard deviation $\sigma_{A,fit}$ from the regression of the NRCan hazard values (NRCan 2015), the standard deviation $\sigma_{Z,seis}$ of the pile settlements predictions, and fi-

Table 5. Pile characteristics considered in this study.

Parameter	Characteristic
Type	Cast in-situ drilled shafts and driven steel pipe piles
Diameter (mm)	350–1200
Length (m)	20–70
Adhesion	Smooth and rough

nally the standard deviation $\sigma_{Z,fit}$ from the regression of $P_{f,a}(a)$ with a lognormal distribution. Assuming that each source of uncertainty is independent, the total uncertainty σ_Z can be expressed as

$$\sigma_Z = \sqrt{\sigma^2_{A,RP} + \sigma^2_{A,fit} + \sigma^2_{Z,seis} + \sigma^2_{Z,fit}} \quad (19)$$

All the terms in eq. (19) are derived as discussed in previous sections.

Results

For the five cities considered in this study, a combination of different pile lengths, cross sections, and types (Table 5) were considered to estimate the probability of failure under seismic loading. First, the fragility functions $F_Z(a)$, obtained through eq. (4), were calculated and shown in Figs. 9*a* and 9*b* for driven piles and drilled shafts, respectively. For each location, fragility functions for three levels of Z_{fail} are shown, each one expressed in terms of percentage of the pile diameters (2%, 5%, and 10%). As expected, at low Z_{fail}, e.g., 2% of the pile diameter, the fragility functions are very steep indicating a very high probability that the limit state (Z <1) is achieved even at modest ground motion intensities. In contrast, for high Z_{fail}, the fragility functions are gentler, indicating a smaller probability that the limit state is achieved. Also, irrespective of the location, drilled piles are more "fragile" than driven piles as indicated by the steeper fragility functions. This is the direct result of using smaller pile resistance parameters β_s and N_t for the drilled shafts suggested by the Canadian Foundation Engineering Manual (Canadian Geotechnical Society 2006) and "softer" load transfer ratios (Reese and O'Neall 1988; CEN 2004*a*). It is interesting to note that at higher ground motion intensities, driven piles and drilled shafts fragility functions are less different, due to the bigger decrease in strength and stiffness caused by large ground motions. For instance, for z_{fail} = 2% and A = 0.4g, a driven steel pile in Vancouver has a probability of failure of 65%, which rises to 82% for drilled piles. For z_{fail} = 2% and A = 0.6g, the probabilities of failure become 85% and 93%, respectively. These results indicate that the use of driven piles is more effective for better seismic performance at small ground motion intensities than at large ground motion intensities.

The unconditional probability of failure $P_{f,1}$ is obtained through to the convolution integral of the fragility function $F_Z(a)$ and the PDF of the ground motion $F_Z(a)$ for every possible $A = a$ (eq. (5)). To directly compare the results of the reliability analysis to the NBC (NRC 2015) reliability target, it is convenient to transform the annual unconditional probability of failure $P_{f,1}$ into an annual reliability index β_1 as

$$\beta_1 = -\Phi^{-1}(P_{f,1}) \quad (20)$$

where Φ^{-1} denotes the inverse standard normal CDF. The relationship between β_1 and the reliability level for a reference period of 50 years, β_{50}, which is the target in NBC (NRC 2015), can be expressed as (Fenton et al. 2016)

$$\beta_1 = \Phi^{-1}\left[\Phi^{1/50}(\beta_{50})\right] \quad (21)$$

Equation (21) applies if each year is considered independent. In NBC (NRC 2015), $\beta_{50,target}$ for ULS is 3 (Bartlett et al. 2003); therefore, applying eq. (21), $\beta_{1,target}$ is equal to 4. Thus, a pile should be designed to experience seismic settlements less than the z_{fail} with a reliability target $\beta_{1,target}$ = 4, for the ULS case. The target SLSs for the seismic case are not specified in NBC (NRC 2015). Following the logic of CHBDC (CSA 2014; Fenton et al. 2016), the target reliability index for the SLS case must be lower than $\beta_{1,target}$ = 4, with a specific value depending on the maximum tolerable settlement needed to achieve or exceed the SLS. The results of the reliability analysis are also compared with the ULS target reliability level for pile groups. $\beta_{50,target,group}$ is less than $\beta_{50,target}$ as failure of one pile does not necessarily imply that the pile group will fail. In this study, $\beta_{50,target,group}$ = 2.33 (TRB 2004) is used; thus, applying eq. (21), $\beta_{1,target,group}$ becomes 3.5.

The results of the convolution integral, eq. (5), are shown in Fig. 10 in terms of the reliability index β_1 as function of Z_{fail} for driven piles in Fig. 10*a* and drilled shafts in Fig. 10*b*. Figure 10 also shows the NBC (NRC 2015) target $\beta_{1,target}$ = 4 and $\beta_{1,target,group}$ = 3.5. Due to the gentler slope of the drilled shafts fragility function, for the same z_{fail}, the driven piles (Fig. 10*a*) achieve higher reliability levels than the drilled shaft (Fig. 10*b*). It is interesting to note that, irrespective of the selected failure settlement z_{fail}, both driven piles and drilled shafts fail to achieve the NBC (NRC 2015) reliability target for a single pile and pile groups. For instance, a 900 mm driven pile in Victoria with a z_{fail} of 6% (z_{fail} = 54 mm) only achieves a seismic reliability β_1 of 2.5. In terms of $P_{f,1}$, using the inverse of eq. (19), the difference between β_1 = 2.5 and β_1 = 4 indicates that each year for that specific pile, the seismic failure is about 200 times more likely than the target. The same pile for a z_{fail} of 10% (90 mm) would have instead an annual seismic failure about 100 times more likely than the target. The authors appreciate that the results presented herein only refer to single piles and that piles in redundant systems would settle less due to the rigidity of the superstructures (Fenton et al. 2016). Nevertheless, the results in Fig. 10 indicate that the difference between the target and the actual performance could be substantial, especially at very low settlements. The reliability analysis of redundant systems under seismic loading is a subject of further research (see Naghibi and Fenton (2017) for an investigation of this topic under static loading).

Simplified procedure for reliability analysis

The pile reliability analysis discussed in the previous sections is quite laborious and its application to every location in a large and diverse country such as Canada would be unpractical. Therefore, the authors propose a simplified procedure that can be used for code calibration studies to derive the geotechnical resistance factors for the seismic design of nonredundant piles. Inspection of Fig. 9 indicates that the pile fragility functions are quite similar at the five different locations when the ground motion is modest and z_{fail} is low. As the ground motion intensity increases and for large z_{fail}, the fragility curves for Victoria and Vancouver become steeper than those for the eastern cities. The reason for this is twofold. First, the national hazard source zone model produces ground motion hazard having different spectral shapes (Adams et al. 2015; Humar 2015). Cities in the east of the country have the maximum spectral response at about 0.1 s whereas the cities in the west have the maximum spectral response at about 0.3 s. As the fundamental period of the site used for this analysis is 0.48 s, the seismic hazard in the west causes larger amplification and excess pore-water pressure than the hazard for the cities in the east. Second, the slope of the ground motion hazard curve $k_{a,1}$ in the west is steeper than the one in the east; therefore, the ground motion values a are larger in the west, for the same mean probability of exceedance, than in the east.

Fig. 9. Fragility curves for (*a*) driven piles and (*b*) drilled shafts.

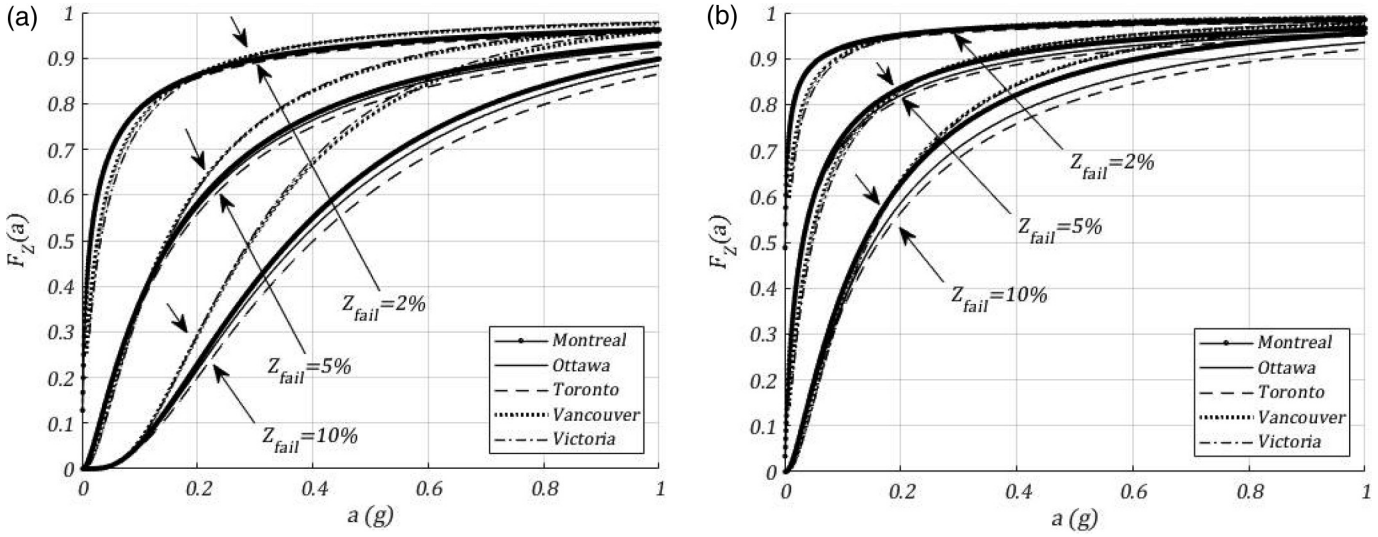

Fig. 10. Reliability levels of pile foundations: (*a*) driven piles and (*b*) drilled shafts.

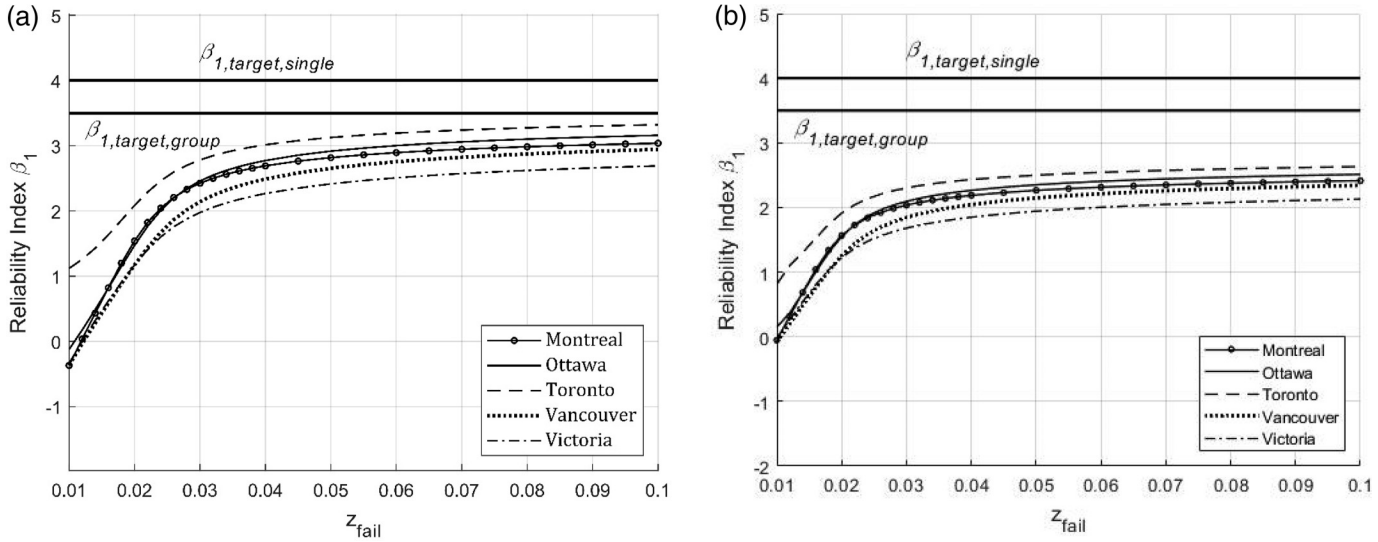

Based on these observations, for the site conditions considered in this study, it seems reasonable to use two sets of generic fragility functions, one for the east and one for the west (Figs. 11*a* and 11*b* for driven piles and Figs. 12*a* and 12*b* for drilled shafts), derived by averaging the limit state function Z from the locations in east and in the west; that is, by grouping the pile settlements in Montreal, Ottawa, and Toronto for the east, and Victoria and Vancouver for the west. The proposed approach is similar to that taken by Luco et al. (2007) and Luco (2009), who introduced a generic fragility function for the seismic design procedures in ASCE 7-16 (ASCE 2016). In addition, the convolution integral in eq. (5) is solved using the approximation introduced by Cornell (1996), which produces an algebraic expression of $P_{f,1}$

$$P_{f,1,s} = H_A(\mu_{\ln Z}) \exp\left[0.5(k_{a,1}\sigma_{\ln Z})^2\right] \quad (22)$$

where H_A is the hazard curve; $k_{a,1}$ is the slope of the hazard obtained from the regression in eq. (6); and $\mu_{\ln Z}$ and $\sigma_{\ln Z}$ are the mean and the standard deviation, respectively, of the natural logarithm of Z defined previously. As Z is lognormally distributed, $\ln(Z)$ is normally distributed and $\mu_{\ln Z}$ corresponds to the median of $\ln(Z)$. Thus, $P_{f,1,s}$ is the product of the hazard curve evaluated at the median capacity of the pile $\mu_{\ln Z}$ times an exponential correction factor that depends on the product of the variability of Z and the slope $k_{a,1}$ of the hazard curve. In effect, eq. (22) is a linearization of the hazard curve $H_A(a)$ in the vicinity of the ground motion corresponding to the median of the fragility function $\mu_{\ln Z}$. Although not demonstrated in this paper, the approximation in eq. (22) is reasonable when the standard deviation of Z, $\sigma_{\ln Z}$, is relatively small and the exponential correction factor is around one order of magnitude (Cornell 1996). As $\sigma_{\ln Z}$ increases, the solution provided by eq. (22) becomes less accurate (Cornell 1996; Hadjan 2004). Use of eq. (22) is possible because $P_{f,1}$ is more sensitive to the slope of the hazard $k_{a,1}$ (and, as a consequence, to the ground motion intensity a) than it is to the value of σ_Z. While the authors recognize that the capacity $F_Z(a)$ and its uncertainty σ_Z can be different for different sites, a single best estimate $\mu_{\ln Z}$ is used herein to represent the pile capacity. As this "single" best estimate of $\mu_{\ln Z}$ is relative to the site conditions and to the ground motion hazards, it may take on different values that depend on the site conditions and to its fundamental period. It could be sufficient to

Fig. 11. Pile fragility functions: (*a*) driven piles west and (*b*) driven piles east.

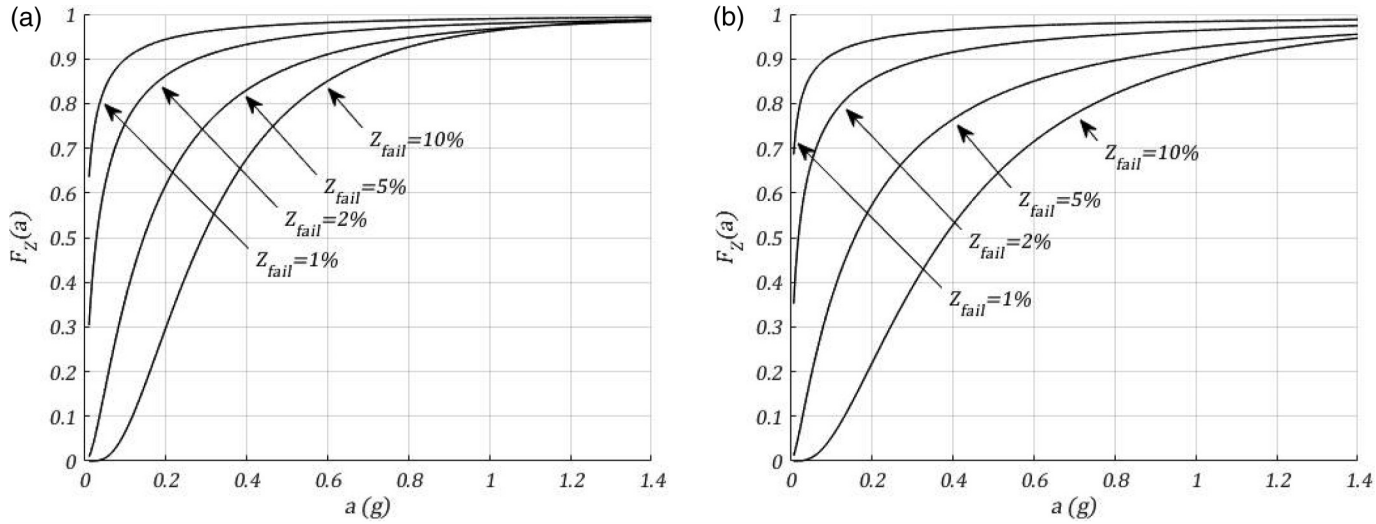

Fig. 12. Pile fragility functions: (*a*) drilled shafts west and (*b*) driven piles east.

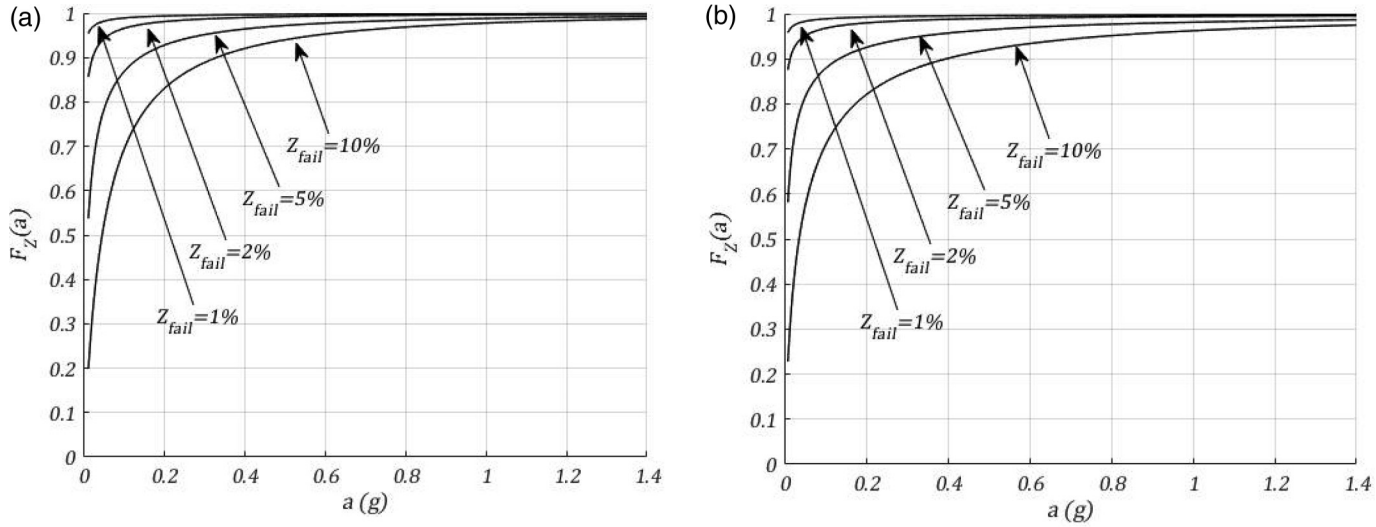

repeat the analysis herein for other site conditions, e.g., site class C, and derive other fragility functions for code calibration.

Equation (22) and the generic fragility functions for east and west of the country (Figs. 11 and 12) are applied to the same five cities considered so far. The simplified $\beta_{1,s}$ versus z_{fail} relationships are shown in Fig. 13. The comparison between the "exact" β_1 and the "simplified" $\beta_{1,s}$ is shown in Fig. 14*a* for driven piles and Fig. 14*b* for drilled shafts as the difference $\beta_1 - \beta_{1,s}$. The similarity between Figs. 10 and 13 and the fact that the difference $\beta_1 - \beta_{1,s}$ is close to 0 for $z_{fail} > 4\%$ of the pile diameter indicates that the approximation produces reasonable results for large z_{fail} corresponding to settlements associated with ULS conditions. Therefore, the simplified approach presented herein could provide an inexpensive approximation for calibration studies. For instance, if a pile is to be designed for a seismic settlement target $P_{f,1,s} \leq P_{f,1,target}$, eq. (22) can inverted so that the pile median capacity, which is the median fragility function μ_{lnZ}, must be (Cornell 1996)

$$\mu_{lnZ} \geq H_A^{-1}(P_{f,1,target}) \exp\left[0.5k_{a,1}\sigma_{lnZ}^2\right] = a \exp\left(0.5k_{a,1}\sigma_{lnZ}^2\right) \quad (23)$$

where $a = H_A^{-1}(P_{f,1,target})$ is the demand ground motion intensity with an exceedance probability equal to $P_{f,1,target}$, which can be derived from eq. (6). Equation (23) states that the median capacity must exceed the design value a by an exponential factor $\exp(0.5k_{a,1}\sigma_{lnZ}^2)$, which is smaller than the exponential factor in eq. (22). The increase in capacity is necessary to accommodate the variability described by σ_{lnZ} and the slope of the ground motion intensity hazard. Thus, if one specifies that, for a particular performance level, the mean frequency of exceedance of the critical settlement level z_{fail} should be, e.g., once in N years, then the appropriate design ground motion intensity a with a mean return period of N years is to be increased by $\exp(0.5k_{a,1}\sigma_{lnZ}^2)$.

Discussion

The authors recognize that the proposed approach to estimate the single pile seismic reliability is a crude approximation of a complex problem. Assumptions were made to extrapolate the ground motion hazard to long return periods and to estimate the variability of the national hazard model. The latter is an important aspect of the seismic reliability and deserves immediate additional attention to allow for more accurate reliability assessments. Also, in this study a simplified 1-D random soil model is used that fails to accurately represent the three-dimensional nature of soil amplification and of the associated excess pore-water

Fig. 13. Reliability levels of pile foundations using eq. (20) and generalized fragility functions: (*a*) driven piles and (*b*) drilled shafts.

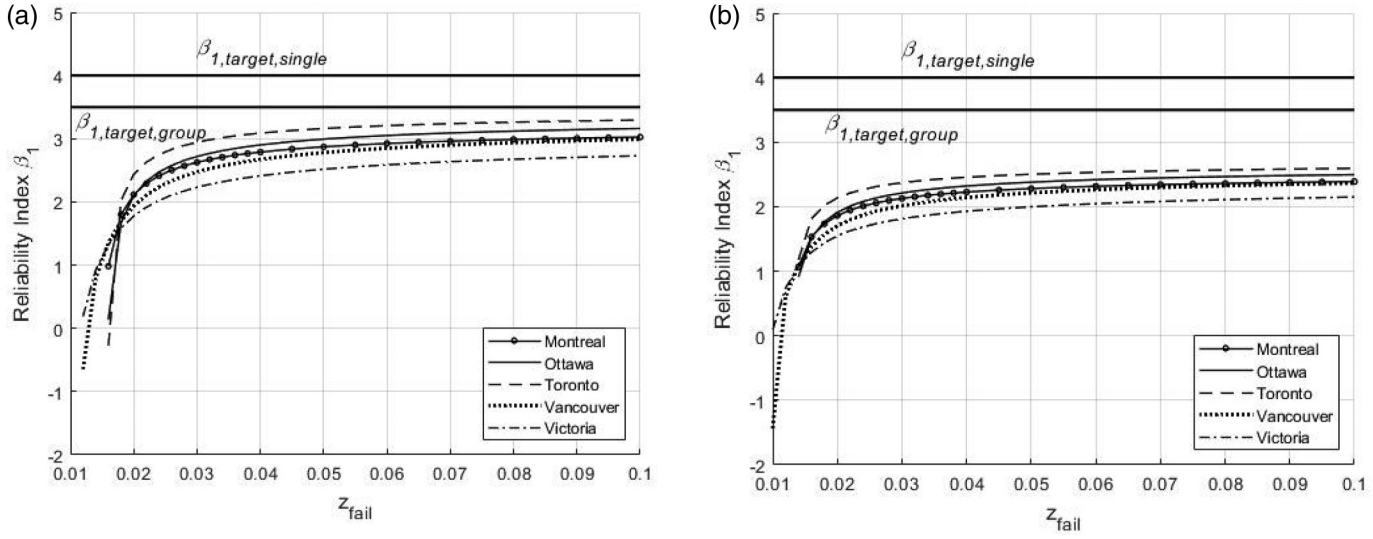

Fig. 14. Comparison of exact and approximate solutions: (*a*) driven piles and (*b*) drilled shafts.

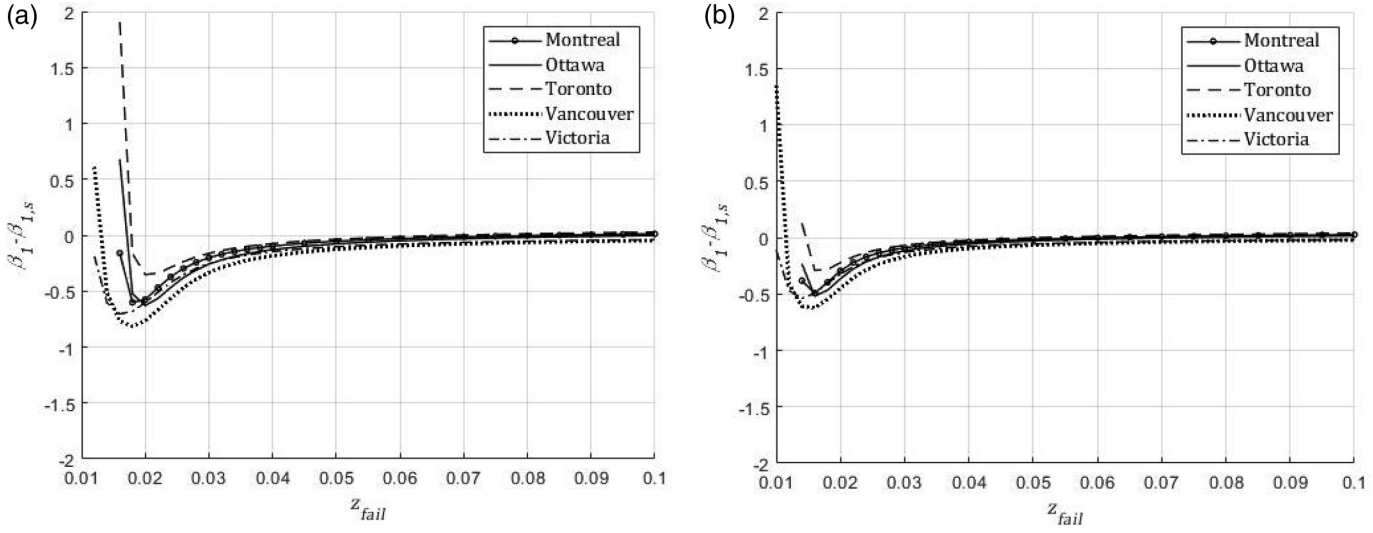

pressure generation and dissipation. Finally, the post-kinematic inertial approach adopted for this study is commonly used in engineering practice, but it fails to properly describe the complex and concurrent occurrence of kinematic and inertial loads.

Therefore, the calculated reliability levels for piles subjected to seismic loads and installed at sites with $v_{s,30}$ = 250 m/s are a necessary simplification of more complex structural systems. Nevertheless, the results presented in the last two sections of this paper offer useful insights concerning the seismic reliability of geotechnical systems. First, the reliability levels calculated with the "exact" convolution integral in eq. (5) and with the simplified procedure of eq. (22) indicate that β_1 reaches a plateau as z_{fail} increases. This indicates that, even for settlements much larger than z_{fail} = 10%, it could be very difficult to achieve the target $\beta_{1,target}$ = 4 of the code. For large z_{fail}, the seismic reliability of driven piles gets closer to the $\beta_{1,target,group}$ of 3.5, indicating that if the effect of the superstructure and structural stiffness are considered, driven pile groups could achieve that reliability level, but only for large settlements leading to the failure of a structure. This implies that even pile foundations of structures able to tolerate very large pile settlements might not be able to achieve the ULS β_1 target prescribed by the code. The correctness of this statement needs to be verified by extending the analysis presented herein to larger z_{fail} values and to redundant foundation systems.

If estimating the settlements able to bring a structure to ULS conditions is a difficult task, it is even more complicated to estimate settlements causing lower levels of damage to a structure. The minimum amount of vertical settlement triggering initiation of structural damage depends on the probability distribution of the resulting angular distortion (relative rotation caused by differential settlements) and on the structural response (Burland et al. 1977) and is not covered in this paper. Nevertheless, it is reasonable to assume that as the amount of settlement increases, the likelihood of structural damage increases from initiation of cracking, and other serviceability issues, to initiation of collapse. The results in Figs. 10 and 13 suggest that the likelihood of seismic-induced serviceability damage associated with small failure settlements z_{fail} could be much higher than what designers, owners, and insurers currently assume, leaving unanswered questions regarding availability and repair costs of structures throughout their design life. For instance, at the site considered in this study, if the settlement initiating serviceability damage is z_{fail} = 2%, driven piles on the west coast of Canada would achieve a reliability level β_1 around 1, corresponding to a $P_{f,1}$ around 16% each year.

Fig. 15. Model variability as function of ground motion intensity.

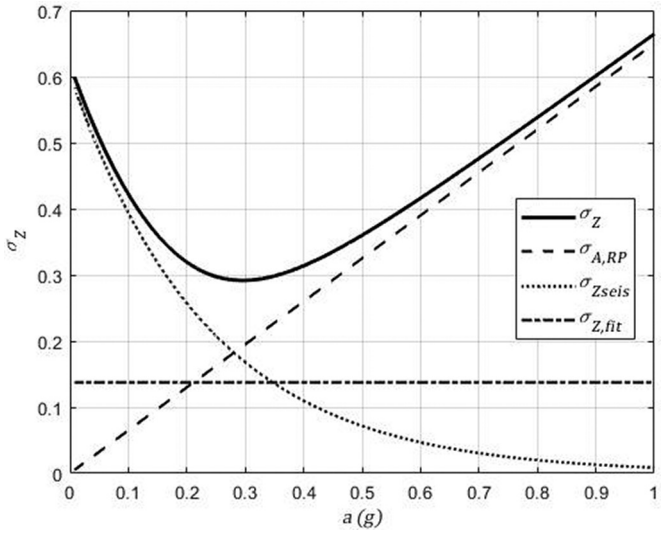

It is important to note that the calculated failure frequencies in this paper are total probabilities of failure that include the possible occurrence of every ground motion intensity in a given year. This is not equivalent to the standard of practice of design for a single MRP ground motion intensity, which instead corresponds to a conditional probability of failure, generally smaller than the total probability of failure. Nevertheless, the calculated failure probabilities seem to be larger than the ones observed in practice, and this raises questions about choices made to model the seismic performance of piles. It was pointed out that the reliability achieved by a pile subjected to seismic loads depends on three parameters: the mean ground motion intensity, a; the slope of the ground motion intensity hazard, $k_{a,1}$; and the total variability of the system, σ_Z, which includes both geotechnical and seismic hazard variability. The mean ground motion intensity, a, and the slope of the ground motion intensity hazard, $k_{a,1}$, are direct outputs of the seismic hazard model. National agencies, such as NRCan that produced the ground motion hazard model used in this study, work continuously to improve their models (Adams and Halchuk 2019). A discussion on how good the model captures the ground motion hazard is not the objective of this paper.

It is instead useful to focus on the total variability σ_Z affecting the calculated reliability levels. When σ_Z increases, $P_{f,1}$ also increases, whereas β_1 decreases. Equation (22) is convenient to estimate the impact of σ_Z on $P_{f,1}$ given the slope of the ground motion hazard $k_{a,1}$. For the same MRE, the same standard deviation σ_Z has a larger impact on the pile reliability where the slope of the ground motion hazard is steeper. Therefore, the same standard deviation σ_Z has more impact on the calculated pile reliability in Victoria and Vancouver where $k_{a,1}$ is larger than in Toronto or Montreal where $k_{a,1}$ is smaller. It is also interesting to understand the contribution to σ_Z from the different standard deviations used in this model (eq. (19)). Figure 15 shows σ_Z as function of the ground motion intensity for z_{fail} = 5% of the pile diameter for a driven pile in Victoria. Figure 15 also shows the contribution of the other sources of variability (see eq. (19)) except $\sigma_{A,fit}$, whose contribution to σ_Z is modest and thus not included in this discussion. Note that for other values of z_{fail} and locations, the shape of the standard deviation curves plotted against the ground motion intensity is similar. Figure 15 indicates that $\sigma_{A,RP}$, which is the standard deviation of the NRCan hazard model (Adams et al. 2015), increases linearly with the ground motion intensity. This is caused by the choice of modelling the variability of the NRCan hazard model (Adams et al. 2015) with a constant $COV_{A,MRP}$ for all MRP at the same location. The standard deviation of the calculated limit state function Z, $\sigma_{Z,seis}$, includes soil variability and geotechnical modelling uncertainty. It decreases as the ground motion intensity increases, as it is expressed as a constant coefficient of variation of Z. Therefore, as the ground motion intensity increases, Z decreases and $\sigma_{Z,seis}$ also decreases. Finally, $\sigma_{Z,fit}$ is the standard deviation of the linear regression of Z versus the ground motion intensity and includes the variability caused by using piles of different geometry in the analysis. As it is calculated as the root mean square of the regression residuals, it remains constant with the ground motion intensity.

Given the variability model adopted in this study, Fig. 15 says that at lower ground motion intensity, the standard deviation σ_Z of the limit state function Z is dominated by the variability of the settlement estimate $\sigma_{Z,seis}$, which represents the geotechnical variability and includes the inherent geological variability of the soil, measurement errors, and model uncertainties. As the ground motion intensity increases, the standard deviation σ_Z of the limit state function Z is dominated by the variability of the NRCan hazard model (Adams et al. 2015) $\sigma_{A,RP}$, which represents the seismological uncertainty including aleatory and epistemic uncertainty (Adams and Halchuk 2019). Thus, for large and rare earthquakes (higher intensity) and large settlements, i.e., the low probability tail of the limit state function Z, the calculated reliability level achieved by piles subjected to seismic loads could be increased if the hazard model uncertainty $\sigma_{A,RP}$ could be somewhat decreased. In contrast, for the higher probability portion of the limit state function Z, i.e., smaller settlements caused by more frequent earthquakes, the reliability level achieved by piles subjected to seismic loads would benefit from a better characterization of the settlements, including more refined site investigation and use of more accurate settlement prediction models.

Finally, the authors believe that the discrepancy between the observed and the calculated performance is also caused by the additional capacity "locked in" the foundation–structure system. The geotechnical system reliability of pile foundations was recently investigated by Naghibi and Fenton (2017) who showed that, depending on degree of correlation of the piles, the system reliability can be much larger than that of a single pile. In addition, there is the capacity provided by the superstructure that further increases the total reliability of the foundation.

Conclusions

In this study, the authors discussed the seismic reliability of nonredundant axially loaded vertical piles installed in a surficial soil deposit with $v_{s,30}$ = 250 m/s and designed according to NBC (NRC 2015) in five major Canadian cities. Also, a simplified reliability approach was proposed based on an algebraic expression of the probability of failure that can be conveniently used for future seismic calibration of Canadian codes. As the seismic performance of axially loaded vertical pile foundations and of the structures they support depends on the load–settlement response, a performance-based approach was used to assess if current geotechnical design practice achieves the target reliability mandated by the NBC (NRC 2015). The authors assumed that the target reliability index for static loads also applies to the seismic design case. The concept of pile failure in terms of limiting settlement was also introduced, which represents the maximum tolerable settlement that the pile can sustain before initiation of damage to the supported structure. As settlement failure can have a broad variety of meanings, ranging from serviceability damage to ultimate limit state, the authors looked at a range of failure settlements defined in terms of percentage of the pile diameter.

The analysis indicates that nonredundant piles designed according to current practice might not be able to achieve the target reliability level prescribed by the NBC (NRC 2015). Even when using the geotechnical resistance factor of the static case, it does not seem possible to achieve the reliability target mandated by

the code. The shortfall is more pronounced for small failure settlements, generally associated with repairable damage, than for large failure settlements, usually associated with initiation of structural collapse. Also, the shortfall is more pronounced in the west of the country than in the east, due to the higher seismicity level in the west and larger variability of the limit state function. Piles associated with small failure settlements have annual probabilities of failure a few orders of magnitude larger than the code target. Piles that can accommodate larger failure settlements are relatively more reliable and have annual probabilities of failure several times (e.g., up to 10 times) larger than the code target.

The analysis presented in this paper is limited to nonredundant single piles; however, structures and their foundation act as systems and possess additional stiffness and strength reserves. When considering the whole structural system, it is possible that pile groups, especially those in the east of the Canada, could get sufficiently close or achieve the target reliability level prescribed by the code due to redundancy. Although this observation regarding redundancy seems somewhat reassuring in terms of public safety, it leaves many questions unanswered regarding availability and repair costs of structures throughout their design life. In particular, the total repair costs from a large earthquake could be higher than what owners, regulators, and insurers are currently assuming.

It is finally recognized that the calculated seismic pile performance seems lower than the observed one. The authors identified a few aspects that should be further investigated to improve the calculation of the reliability level achieved by a pile foundation under seismic loads. The uncertainty associated with the settlement calculation model and with the ground motion hazard model is very large and decreases the calculated reliability level of nonredundant piles subject to seismic load conditions. Both are important aspects of the reliability calculation that deserve immediate attention.

References

AASHTO. 2017. AASHTO bridge design specifications. American Association of State Highway and Transportation Officials (AASHTO), Washington, D.C.

Adams, J., and Halchuk, S. 2019. Uncertainty spread in the 5th generation seismic hazard results used in NBCC 2015. *In* Proceedings of 12th Canadian Conference on Earthquake Engineering, Quebec City, 17-20 June 2019.

Adams, J., Halchuk, S., Allen, T.I., and Rogers, G.C. 2015. Canada's 5th generation seismic hazard model, as prepared for the 2015 National Building Code of Canada. *In* Proceedings of the 11th Canadian Conference on Earthquake Engineering, Victoria, BC. Paper No. 93775.

Anderson, D.L., Byrne, P.M., DeVall, R.H., Naesgaard, E., and Wijewickreme, D. 2007. Task Force Report - Geotechnical design guidelines for buildings on liquefiable sites in Greater Vancouver in accordance with NBCC 2005. Greater Vancouver Seismic Geotechnical Design Task Force, Vancouver, BC.

Argyroudisa, S., Kayniabc, A.M., and Pitilakisa, K. 2013. Development of fragility functions for geotechnical constructions: application to cantilever retaining walls. Soil Dynamics and Earthquake Engineering, **50**(3): 106–116. doi:10.1016/j.soildyn.2013.02.014.

ASCE. 2016. Minimum design loads for buildings and other structures. American Society of Civil Engineering (ASCE)/SEI, Reston, Va.

Bartlett, F.M., Hong, H.P., and Zhou, W. 2003. Load factor calibration for the proposed 2005 edition of the National Building Code of Canada: Companion-action load combinations. Canadian Journal of Civil Engineering, **30**(2): 440–448. doi:10.1139/L02-086.

Bazzurro, P., and Cornell, A.C. 2004*a*. Ground-motion amplification in nonlinear soil sites with uncertain properties. Bulletin of the Seismological Society of America, **94**(6): 2090–2109. doi:10.1785/0120030215.

Bazzurro, P., and Cornell, A.C. 2004*b*. Nonlinear soil-site effects in probabilistic seismic-hazard analysis. Bulletin of the Seismological Society of America, **94**(6): 2110–2123. doi:10.1785/0120030216.

Burland, J.B., Broms, B.B., and De Mello, V.F.B. 1977. Behaviour of foundation and structures. *In* Proceedings of the IX ICSMFE Conference, Tokyo, Japan.

CEN. 2004*a*. EN 1997:2004: Eurocode 7 – Geotechnical design. European Committee for Standardization (CEN), Brussels, Belgium.

CEN. 2004*b*. EN 1998:2004: Eurocode 8 – design of structures for earthquake resistance - Part 5: Foundations, retaining structures and geotechnical aspects. European Committee for Standardization (CEN), Brussels, Belgium.

Canadian Geotechnical Society. 2006. Canadian Foundation Engineering Manual. Bitech Publisher Ltd., Richmond, B.C.

Cornell, A.A. 1996. Calculating building seismic performance reliability. a basis for multi-level design norms. *In* Proceedings of Eleventh World Conference on Earthquake Engineering, Elsevier Science, Rotterdam, the Netherlands.

CSA. 2014. S6-14 Canadian Highway Bridge Design Code. Canadian Standards Association (CSA), Toronto, Ont.

CSA. 2019. S6-19 Canadian Highway Bridge Design Code. Canadian Standards Association (CSA), Toronto, On.

Cubrinovski, M., and Rees, S. 2008. Effects of fines on undrained behaviour of sands. *In* Proceedings of ASCE, Geotechnical Earthquake Engineering and Soil Dynamics Congress IV, Sacramento, California, United States.

Cubrinovski, M., Rees, S., and Bowman, E. 2010. Effects of non-plastic fines on liquefaction resistance of sandy soils. *In* Earthquake engineering in Europe. *Edited by* M. Garewski, A., Ansal, Springler Science, Berlin, Germany.

Dutch Institute for Standardization. 2006. Dutch Standard NEN 6743-1:2006 Geotechnics - Calculation method for bearing capacity of pile foundation - Compression piles. Dutch Institute for Standardization, Amsterdam, the Netherlands. [In Dutch.]

Esposito, G. 2017. Effectiveness of blow-count to assess the serviceability reliability of a high-speed train piled foundation. *In* Proceeding of GeoOttawa 2017, Canadian Geotechnical Society, Ottawa, ON.

Fenton, G.A., and Griffiths, D.V. 2003. Bearing-capacity prediction of spatially random c–ϕ soils. Canadian Geotechnical Journal, **40**(1): 54–65. doi:10.1139/t02-086.

Fenton, G.A, Naghibi, F., Dundas, D., Bathurst, R.J., and Griffiths, D.V. 2016. Reliability-based geotechnical design in 2014 Canadian Highway Bridge Design Code. Canadian Geotechnical Journal, **53**(2): 236–251. doi:10.1139/cgj-2015-0158.

Galbraith, J.A., Ali Naeem, M., and Bruin, W.M. 2018. Evaluation of marine structures for kinematic effects. *In* Proceedings of PIANC-World Congress Panama City, PIANC, Panama.

Green, R.A., and Terri, G.A. 2005. Number of equivalent cycles concept for liquefaction evaluations–revisited. Journal of Geotechnical and Geoenvironmental Engineering, **131**(4): 477–488. doi:10.1061/(ASCE)1090-0241(2005)131:4(477).

Hadjan, A. 2004. Earthquake reliability of structures. *In* Proceeding of the 13th World Conference on Earthquake Engineering, Vancouver, B.C., Canada.

Honjo, Y., Suzuki, M., Shirato, M., and Fukui, J. 2004. Determination of partial factors for a vertically loaded pile based on reliability analysis. *In* Proceeding of IWS Kamakura. pp. 297–303.

Humar, J. 2015. Background to some of the seismic design provisions of the 2015 National Building Code of Canada. Canadian Journal of Civil Engineering, **42**(11): 940–952. doi:10.1139/cjce-2014-0385.

Kottke, A.R., and Rathje, E.M. 2008. Technical manual for Strata. Report No.: 2008/10. Pacific Earthquake Engineering Research Center, University of California, Berkeley, CA.

Kramer, S.L., Valdez, C., Blanchette, B., and Baker, J.W. 2014. Performance-based design factors for pile foundations. WSDOT Research Report, WA-RD 827.1, Seattle, Wash.

Lasley, S.J., Russell, A.G., and Rodriguez-Marek, A. 2017. Number of equivalent stress cycles for liquefaction evaluations in active tectonic and stable continental regimes. Journal of Geotechnical and Geoenvironmental Engineering, **143**(4): 161–171. doi:10.1061/(ASCE)GT.1943-5606.0001629.

Luco, N. 2009. Preparation of new seismic design maps for building codes. *In* Proceedings of 2009 COSMOS, Consortium of Organizations for Strong-Motion Observation Systems, San Francisco, Calif.

Luco, N., Ellingwood, B.R., Hamburger, R.O., Hooper, J.D., Kimball, J.K., and Kircher, C.A. 2007. Risk-targeted versus current seismic design maps for the conterminous United States. *In* Proceedings of SEAOC 2007 Convention, Squaw Creek, Calif.

Naghibi, F., and Fenton, G.A. 2017. Target geotechnical reliability for redundant foundation systems. Canadian Geotechnical Journal, **54**(7): 945–952. doi:10.1139/cgj-2016-0478.

Naghibi, F., and Fenton, G.A. 2019. Calibration of resistance factors for geotechnical seismic design. Canadian Geotechnical Journal, **56**(8): 1134–1141. doi:10.1139/cgj-2018-0433.

NRC. 2005. National Building Code of Canada. National Research Council Canada (NRC), Ottawa, Ont.

NRC. 2015. National Building Code of Canada. National Research Council Canada (NRC), Ottawa, Ont.

NRCan. 2015. Online hazard calculator. Natural Resources Canada (NRCan). Available from http://www.seismescanada.rncan.gc.ca/hazard-alea/interpolat/index-en.php.

Oregon Department of Transportation. 2018. Geotechnical design manual. Chapter 6 – Seismic design. Oregon Department of Transportation, Portland, OR.

Polito, C.P., Green, R.A., and Lee, J. 2008. Pore pressure generation models for sands and silty soils subjected to cyclic loading. Journal of Geotechnical and Geoenvironmental Engineering, **134**(10): 1123–1141. doi:10.1061/(ASCE)1090-0241(2008)134:10(1490).

Reese, L.C., and O'Neill, M. 1988. Criteria for design of axially loaded drilled shafts. Center for Highway Research Report, University of Texas, Austin, TX.

Seed, H.B., Idriss, I.M., Makdisi, F., and Banerjee, N. 1975. Representation of irregular stress time histories by equivalent uniform stress series in liquefac-

tion analyses. EERC Report 75-29, Earthquake Engineering Research Center, University of California, Berkeley, Calif.
Toro, G.R. 1995. Probabilistic models of site velocity profiles for generic and site-specific ground-motion amplification studies. Brookhaven National Laboratory Report, New York, N.Y.

List of symbols

A ground motion intensity (random)
A_t pile toe area
a ground motion intensity
b_i regression coefficients for N_{eq}
C pile circumference
c_i regression coefficients for r_u
COV coefficient of variation
$COV_{A,MRP}$ coefficient of variation of $A = a$ at return period MRP
COV_R coefficient of variation of the static geotechnical axial capacity R
$COV_{Z,fit}$ coefficient of variation of the linear regression of Z
$COV_{Z,seis}$ coefficient of variation of the geotechnical seismic model
$COV_{Z_{transfer}}$ coefficient of variation of the load-transfer ratio
CSR cyclic stress ratio
Dr relative density
d depth of soil layer
$F_A(a)$ cumulative density function (CDF) of ground motion intensity
FC fines contents
$F_Z(a)$ fragility function
$F_{Z,a}$ fragility of the pile at the ground motion $A = a$
f_A probability density function (PDF) of ground motion intensity
f_Z probability density function of Z
H_A complementary cumulative distribution function (CCDF) of ground motion intensity
$H_A^{-1}()$ inverse of the ground motion intensity CCDF
h expected soil layer thickness
$k_{a,i}$ regression coefficients of H_A vs a
$k_{d,i}$ coefficients of nonhomogeneous Poisson process
$k_{Z,i}$ coefficients of limit state regression
L pile axial load
L_{des} factored axial load
L_{fail} failure load
L_{pile} pile length
L_{seis} seismic axial load
L_{ult} ultimate pile axial capacity
M_w moment magnitude
MRE annual mean rate of exceedance
MRP mean return period
N number of years
N_{eq} number of equivalent cycles
N_{liq} number of equivalent cycles to liquefaction
N_t bearing capacity factor
P[] probability of failure
PDF probability density function
$P_{f,1}$ annual total probability of failure
$P_{f,a}$ conditional probability of pile failure
$P_{f,1,s}$ simplified annual total probability of failure
$P_{f,1,target}$ target annual total probability of failure
PGA peak ground acceleration
q_s shear stress along shaft
q_t bearing capacity of pile toe
R geotechnical axial capacity of pile
r_u pore-water pressure ratio
S_i standard normal variable of property X of soil layer i
s'_v vertical effective stress
$s'_{v,seis}$ seismic vertical effective stress
u pore-water pressure
$v_{s,30}$ mean shear velocity of top 30 m
W_p pile weight
X property of soil layer (density, shear-wave velocity or damping)
X_i soil property in ith layer
Z limit state function of settlements (random)
Z_{fail} failure settlement (random)
Z_{seis} seismic settlement (random)
z limit state settlements
z_{des} design settlement
z_{fail} failure settlement
z_{seis} seismic settlement
z_{ult} ultimate settlement
α empirical constant for pore pressure calculation
β reliability index
β_1 annual reliability index
β_{50} reliability index for reference period of 50 years
$\beta_{1,target}$ annual target reliability index
$\beta_{50,target}$ target reliability index for a reference period of 50 years
$\beta_{50,target,group}$ target reliability index for pile groups
$\beta_{50,target,single}$ target reliability index for single pile
β_s shaft resistance factor
δ_0 residual term of N_{eq} regression
Δz segment of pile length
ε_i normal random variable with zero mean and unit standard deviation
$\lambda(d)$ rate of Poisson process used to model soil variability
μ_H mean of ground motion intensity CCDF
μ_{lnX} mean of the natural logarithm of the soil property
μ_{lnZ} mean of the natural logarithm of Z
μ_{r_u} mean of increase in pore pressure
μ_Z mean value of Z
$\mu_{Z,seis}$ mean of seismic settlement
ρ correlation coefficient between adjacent layers
$\sigma_{A,MRP}$ standard deviation of $A = a$ at the return period MRP
$\sigma_{A,fit}$ standard deviation of $A = a$ from NRCan model
$\sigma_{A,RP}$ standard deviation of NRCan hazard model
σ_H standard deviation of ground motion intensity CCDF
σ_{lnX} standard deviation of the natural logarithm of the soil property
σ_{lnZ} standard deviation of the natural logarithm of Z
$\sigma_{N_{eq}}$ standard deviation of N_{eq}
$\sigma_{N_{liq}}$ standard deviation of N_{liq}
σ_{r_u} standard deviation of increase in pore pressure
σ_Z standard deviation of Z
$\sigma_{Z,fit}$ standard deviation of Z regression
$\sigma_{Z,seis}$ standard deviation of seismic settlement
$\Phi[]$ standard normal CDF
Φ^{-1} inverse standard normal CDF
φ geotechnical resistance factor